What is the (Dark) Matter with Dwarf Galaxies?

Till Sawala[1]*, Qi Guo[3], Cecilia Scannapieco[2], Adrian Jenkins[3] and Simon White[1]

[1] *Max-Planck Institute for Astrophysics, Karl-Schwarzschild-Strasse 1, 85748 Garching, Germany*

[2] *Astrophysikalisches Institut Potsdam, An der Sternwarte 16, 14482 Potsdam, Germany*

[3] *Institute for Computational Cosmology, Department of Physics, University of Durham, South Road, Durham DH1 3LE, UK*

ABSTRACT

We present cosmological hydrodynamical simulations of the formation of dwarf galaxies in a representative sample of haloes extracted from the Millennium-II Simulation. Our six haloes have a $z = 0$ mass of $\sim 10^{10} M_\odot$ and show different mass assembly histories which are reflected in different star formation histories. We find final stellar masses in the range $5 \times 10^7 - 10^8 M_\odot$, consistent with other published simulations of galaxy formation in similar mass haloes. Our final objects have structures and stellar populations consistent with observed dwarf galaxies. However, in a ΛCDM universe, $10^{10} M_\odot$ haloes must typically contain galaxies with much lower stellar mass than our simulated objects if they are to match observed galaxy abundances. The dwarf galaxies formed in our own and all other current hydrodynamical simulations are more than an order of magnitude more luminous than expected for haloes of this mass. We discuss the significance and possible implications of this result.

Key words: cosmology: theory – galaxies: dwarf – galaxies: formation – galaxies: evolution – galaxies: luminosity function, mass function – methods: N-body simulations

1 INTRODUCTION

Dwarf galaxies are by far the most abundant type of galaxy in the Local Group and in the Universe. They span a large range of stellar masses, morphologies and star formation histories. The largest dwarf irregulars such as the large Magellanic Cloud have stellar masses of $\sim 10^9 M_\odot$, rotationally supported and HI-rich disks, and strong ongoing star formation. In contrast, dwarf spheroidal galaxies have stellar masses from $10^7 M_\odot$ to below $10^3 M_\odot$, they possess no interstellar gas, and they show no sign of rotational support or ongoing star formation.

The number of dwarf galaxies observed in the Local Group continues to grow as new, 'ultra-faint' satellite galaxies are discovered (e.g. Martin et al. 2006; Chapman et al. 2007; Belokurov et al. 2010). Estimates using luminosity functions corrected for completeness and bias predict the total number of faint satellites to be an order of magnitude higher still (Tollerud et al. 2008; Koposov et al. 2008). Nevertheless, this is still much smaller than the total number of dark matter subhaloes found in high-resolution simulations of the standard ΛCDM cosmology (e.g. Klypin et al. 1999; Moore et al. 1999; Diemand et al. 2007; Springel et al. 2008). This difference has become known as the "Missing Satellites Problem". It may only be an apparent discrep-

ancy, however, since it can be removed if one accounts for the fact that not all low-mass subhaloes must contain stars, and those that do may have very high mass-to-light ratios. Several astrophysical mechanisms have been suggested that can lead to a number of visible satellite galaxies similar to that observed. Perhaps haloes were able to form a few stars initially, but the baryonic components of all haloes below some critical mass were subsequently destroyed by supernova feedback (e.g. Larson 1974; Dekel & Silk 1986; Ferrara & Tolstoy 2000). Alternatively (or perhaps additionally) photoionisation may have prevented star formation in the smallest haloes (e.g. Efstathiou 1992; Somerville 2002; Hoeft et al. 2006; Simon & Geha 2007). As Sawala et al. (2010) have shown, these two mechanisms can combine to produce very high mass-to-light ratios in haloes of $10^9 M_\odot$ and below, perhaps reconciling the number of very faint dwarf galaxies produced in ΛCDM simulations with the observations.

In this work, we turn our focus to more massive dwarf galaxies, and follow the evolution of the objects that form in haloes of $10^{10} M_\odot$. Our initial conditions are based on six haloes selected from the Millennium-II Simulation (MS-II, Boylan-Kolchin et al. 2009), and resimulated at high resolution using smoothed particle hydrodynamics (SPH). Our simulations include cooling and star formation, supernova feedback, metal-enrichment and a cosmic UV background. Starting at redshift $z = 49$, we are able to follow the forma-

* E-Mail: till@mpa-garching.mpg.de

tion of each individual halo and its central galaxy in their full cosmological context, all the way to $z = 0$.

On the other hand, the large volume of our parent simulation allows us to verify that our sample of resimulated haloes is representative of haloes of similar mass, and to predict a stellar mass – halo mass relation that can be tested against observation. With a box size of 137 Mpc and a mass resolution of $9.4 \times 10^6 M_\odot$, the MS-II has sufficient dynamic range to capture the statistics of the assembly of dark matter haloes between 10^9 and $10^{14} M_\odot$. By comparing its halo/subhalo mass function to the observed SDSS stellar mass function of Li & White (2009), Guo et al. (2010) derived a typical mass-to-light ratio for each halo mass. This analysis assumes a monotonic relationship between halo mass and galaxy mass with relatively small scatter, but does not rely on any other assumptions about the processes involved in galaxy formation. We use its result to test the viability of our simulations and the underlying physical model as a description of the formation of "typical" ΛCDM dwarf galaxies.

The present work constitutes the first direct comparison of high resolution, hydrodynamical simulations of individual dwarf galaxies with the observed abundance of such objects. We combine the ability to follow star formation self-consistently in individual objects with the ability to draw conclusions about the general population of dwarf galaxies.

This paper is organised as follows: We begin in Section 2 by reviewing the current status of simulations of the formation of dwarf galaxies. Section 3 describes the selection of haloes for resimulation and the generation of our high resolution initial conditions, while the numerical methods of our hydrodynamic simulations are discussed briefly in Section 4. In Section 5, we show results for six haloes of final mass $10^{10} M_\odot$, and compare the properties of the galaxies to previous work, and to observation. In Section 6, we consider the predictions of our simulations for the stellar mass – halo mass relation and discuss the discrepancy with that inferred from comparing the observed stellar mass function to the halo abundance in ΛCDM simulations. We conclude with a summary and interpretation of our results in Section 7.

Unless stated otherwise, where we refer to the mass of a *galaxy*, we mean the stellar mass $M_\star$, whereas the mass of a *halo* includes the total dynamical mass enclosed within r_{200}, the radius that defines a spherical overdensity 200 times the critical density of the universe. When quoting the results for our own simulations, we always use physical mass units of $M_\odot$, assuming h = 0.73.

2   REVIEW OF PREVIOUS WORK

Earlier examples of numerical studies of dwarf galaxy formation and evolution in $\sim 10^{10} M_\odot$ haloes include simulations by Pelupessy et al. (2004), Stinson et al. (2007, 2009), Valcke et al. (2008), Mashchenko et al. (2008) and Governato et al. (2010).

The first three have investigated the evolution of dwarf galaxies embedded in dark matter haloes of constant mass. Pelupessy et al. used initial conditions modelled after dwarf irregular galaxy DDO 47, set up with a stellar disk of

**Table 1.** Results of earlier numerical simulations

Reference	$M_\star$ [$10^7 M_\odot$]	M_{tot} [$10^9 M_\odot$]	v_c or $\sigma_\star$ [km s^{-1}]
Pelupessy et al. (2004)[1]	18	15	80
Stinson et al. (2007)[2]	7.86	5.0	15.1
Stinson et al. (2007)[2]	22	8.6	20.1
Stinson et al. (2007)[2]	38.6	14	29.9
Stinson et al. (2009)[3]	1.72	14	16.8
Valcke et al. (2008)[4]	57.9	4.1	35.2
Valcke et al. (2008)[4]	48.8	4.1	30.9
Mashchenko et al. (2008)[5]	1.0	2.0	–
Governato et al. (2010)[6]	48	35	56
Governato et al. (2010)[6]	18	20	54

Notes: Col. 2: Stellar mass, Col. 3: Halo mass (M_{200}), Col. 4: Maximum rotation velocity[1,6] or 1-D velocity dispersion[2,3,4]. All quantities are measured at $z = 0$, except for Mashchenko et al., where the halo mass is at $z = 5$ and stellar mass at $z = 6.2$. Remarks: [1]Static initial conditions set up to reproduce the dwarf irregular galaxy DDO 47; [2,3]Static NFW profiles with initial baryon fractions of 10%[2] and 1%[3]; [4]Runs DH01 and DH02, assuming static, simplified Kuz'min Kutuzov profiles with $a = c = 4$ kpc (DH01) and 6 kpc (DH02).

$1.8 \times 10^8 M_\odot$ and a gas disk of $1.9 \times 10^8 M_\odot$ inside a dark matter halo of $1.5 \times 10^{10} M_\odot$. Thus, the stellar mass to halo mass ratio is not a result of their simulation, but was chosen *a priori*. They show that the star formation behaviour in such a system is consistent with observations. Valcke et al. studied the formation of dwarf elliptical galaxies assuming cored initial dark matter profiles following Dejonghe & de Zeeuw (1988), and gas at a mass fraction of 17.5%. Cooling, star formation and feedback are included in their simulations, making their final stellar masses of $4.9 - 5.8 \times 10^8 M_\odot$ for haloes of $4.1 \times 10^9 M_\odot$ a direct prediction of their models. Stinson et al. also assume fixed dark matter profiles in their initial conditions, and perform simulations that include cooling, star formation and feedback. In Stinson et al. (2007), a fixed initial baryon fraction of 10% is assumed, and stellar masses of $7.9 \times 10^7 - 3.9 \times 10^8 M_\odot$ are produced in haloes of $5 \times 10^9 - 1.4 \times 10^{10} M_\odot$. In Stinson et al. (2009), the baryon fraction is varied, and we also include their result with a very low initial baryon fraction of 1%, that leads to a smaller stellar mass. Valcke et al. and Stinson et al. do not include a UV background, which may contribute to the high star formation efficiency in their simulations.

Mashchenko et al. (2008) and Governato et al. (2010) both performed simulations that include the formation of the dark matter halo in a cosmological volume. Mashchenko et al. used constrained initial conditions, aimed at reaching a halo mass of $10^9 M_\odot$ at $z = 6$, and followed the evolution up to $z = 5$. At this time, their halo reached a mass of $2 \times 10^9 M_\odot$, with $10^7 M_\odot$ of stars formed. By comparison with the typical evolution of haloes in the MS-II (see Figure 2), we note that this is consistent with a mass of $10^{10} M_\odot$ at $z = 0$. The extent of additional star formation up to $z = 0$ is unknown, however. Most recently, Governato et al. have performed hydrodynamical simulations of two dwarf irregular galaxies at very high resolution, which they follow up to $z = 0$. This makes these most comparable to our own simulations, and also makes their results most directly comparable to observed, present-day dwarf galaxies. Their simulations
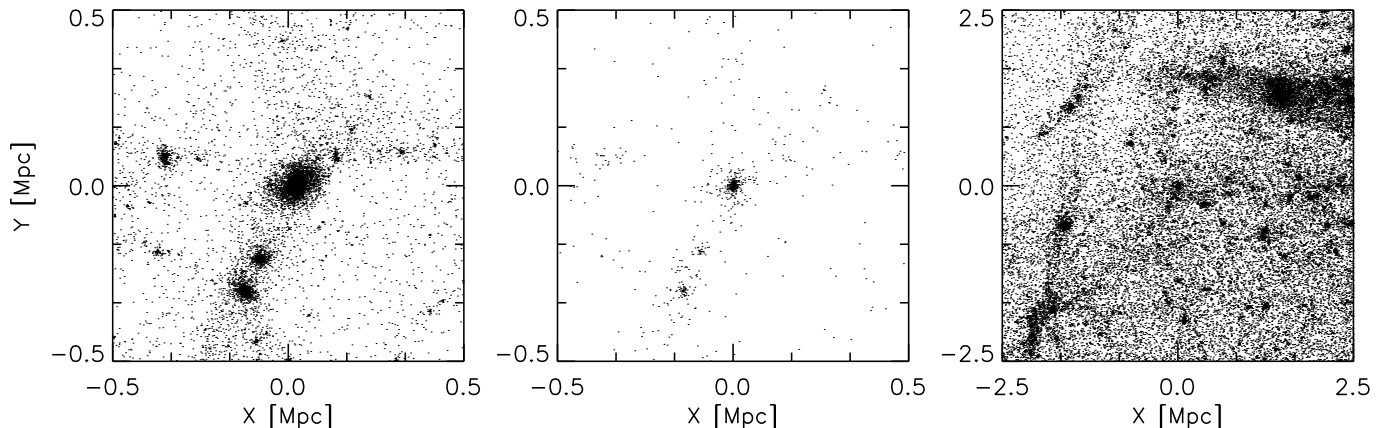
Figure 1. Comparison of Halo 4 at $z = 0$ in a pure dark matter resimulation and in the parent Millennium-II Simulation. The left panel shows the position of 0.5% of the particles in a box of sidelength 1 Mpc in the resimulation, while the central panel shows the position of all particles within the same region in the MS-II. The panel on the right shows all particles in a box of 5 Mpc in the MS-II, with Halo 4 in the centre. All three panels are centred on the same absolute coordinates for the parent box of sidelength 137 Mpc, showing the position of the halo to be in perfect agreement. The FoF mass of the halo also agrees to within less than 1%. A comparison of the left and the central panel reveals the additional substructure resolved in the resimulation.

start with values of $\Omega_\mathrm{m} = 0.24$, $\Omega_\mathrm{b} = 0.042$, and predict stellar masses of 1.8 and $4.8 \times 10^8 \mathrm{M}_\odot$ in two haloes of 2.0 and $3.5 \times 10^{10} \mathrm{M}_\odot$, respectively.

While these five sets of simulations vary in the setup of the initial conditions, the cooling, star formation and feedback recipes, the treatment of the cosmic UV background, the simulation code and the numerical resolution, they all predict final stellar masses consistent with $\sim 10^8 \mathrm{M}_\odot$ for dark matter haloes of $\sim 10^{10} \mathrm{M}_\odot$. We give an overview of some of the relevant properties of these simulations in Table 1.

3 INITIAL CONDITIONS

The parent simulation, as well as our high-resolution resimulations, are performed in the context of a ΛCDM cosmology, with $\Omega_\Lambda = 0.75$, $\Omega_\mathrm{m} = 0.25$, h= 0.73 and $\sigma_8 = 0.9$, identical to the values used for the original Millennium Simulation (Springel et al. 2005).

The Millennium-II Simulation followed structure formation in a volume of 137^3 Mpc^3 using 2160^3 dark matter particles and periodic boundary conditions. This corresponds to a mass resolution of $9.43 \times 10^6 \mathrm{M}_\odot$, and a force resolution of 1.37 kpc. At $z = 0$, it contains about 12 million friends-of-friends (FoF) haloes with at least 20 particles, corresponding to a minimum resolved halo mass of $1.9 \times 10^8 \mathrm{M}_\odot$. Haloes of $\sim 10^{10} \mathrm{M}_\odot$, the mass at $z = 0$ that we select for our resimulations, are resolved with over 10^3 particles.

Out of more than 10^4 haloes within our mass range in the MS-II, we identified 25 haloes as resimulation candidates, based on the condition that all particles within twice the virial radius at redshift $z = 0$ were in a connected region and inside a sphere of radius 0.67 Mpc in the initial conditions. Out of these, six haloes were selected in order to study a varied but representative sample of mass accretion histories (see Figure 2). The initial conditions for the resimulations were generated by re-sampling the region of interest with a high number of low mass dark matter particles, while the remaining volume was sampled with increasingly coarser resolution, sufficient to capture the long-range

tidal field. To account for the higher Nyquist frequency of the resimulations, small-scale fluctuations were added to the displacement and velocity fields of the original MS-II using the method of second-order Lagrangian perturbation theory described in Jenkins (2010).

Figure 1 shows the final distribution of dark matter particles in slices centred on a dwarf halo in the MS-II and in one of our high-resolution resimulations (pure dark matter). The difference in mass between the central FoF halo in the resimulations and in the MS-II is $< 1\%$, equivalent to ~ 10 particles in the parent simulation. The position and velocity are well reproduced, and the agreement also extends to substructures outside the main halo. The structure resolved in the MS-II is again found at the correct mass and location, while some additional substructure is visible only in the resimulation.

We have performed resimulations both with pure dark matter and with gas particles added, splitting each high-resolution dark matter particle at a mass ratio of $\Omega_\mathrm{b} = 0.046$ to $\Omega_\mathrm{DM} = 0.204$. All resimulations start at $z = 49$ and are evolved up to $z = 0$. The hydrodynamical simulations include 1.1×10^6 high resolution dark matter particles of $8 \times 10^4 \mathrm{M}_\odot$, and an equal number of gas particles of $1.8 \times 10^4 \mathrm{M}_\odot$. The initial stellar particle mass is $9 \times 10^3 \mathrm{M}_\odot$. At $z = 0$, the individual haloes are resolved with more than 10^5 particles within r_{200}. The volume outside of the high-resolution region is sampled with an additional 7.6×10^5 dark matter particles of varying mass to include the evolution of structure on large scales.

To check for possible biases due to our selection method, we have compared our candidates for resimulation to the total population of similar mass haloes in the MS-II. Figure 2 shows as solid lines the merger histories of the six selected dark matter haloes in the high resolution simulations, together with the typical mass accretion history, derived from merger trees of $\sim 10^4$ randomly selected, similar mass haloes. At each redshift, the inner and outer grey regions indicate the 3rd, 16th, 84th and 97th percentiles, equivalent to 1σ and 2σ deviations from the mean mass for
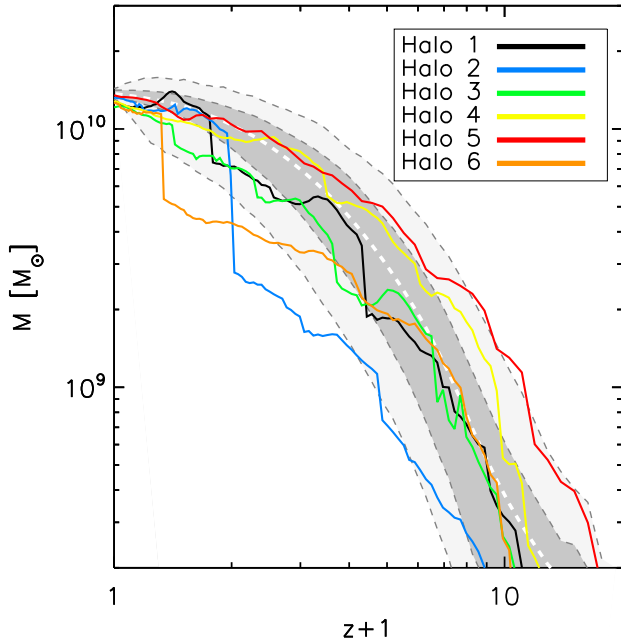
Figure 2. Evolution of FoF-halo mass as a function of redshift in our pure dark matter resimulations. The solid coloured lines show the mass accretion history of the six haloes we have resimulated at high resolution. Overplotted as a thick dashed line is the mean halo mass from the Millennium-II Simulation, for all haloes of similar final masses. Also shown are the 1σ and 2σ upper and lower bounds at each redshift, in dark and light shades, respectively. It can be seen that there is a variety of assembly histories, both in the parent simulation, and in the sample of resimulated haloes. Haloes 3 and 6 have undergone recent major mergers, while Halo 5 formed significantly earlier than the five others. The variety within our sample is somewhat greater than expected for a random sub-sample of the MS-II, but there is no systematic bias in formation history. Formation redshifts, defined as the time when a halo reaches half its peak mass, lie between 1 and 2.5, consistent with a median formation redshift of 2. Note that the halo mass m_{200} can differ from the FoF-mass by $\sim 5 - 15\%$, and due to outflows, the total mass in each of the six haloes is reduced to $\sim 10^{10} M_{\odot}$ in the resimulations with gas.

a Gaussian mass distribution. It can be seen that the variance within our sample is higher than the expected variance within a random sub-sample of haloes. This allows us to follow the evolution of haloes with a range of merger histories in a limited number of simulations. However, there is no systematic bias in the mass accretion history of our haloes, so our sample can be considered a reasonably unbiased representation of $10^{10} M_{\odot}$ haloes in the MS-II.

4   NUMERICAL METHODS

The high-resolution simulations presented here have been performed using the Tree-PM code GADGET-3 (Springel 2005; Springel et al. 2008), which includes gravity and smoothed particle hydrodynamics. As an extension, metal-dependent cooling, star formation, chemical enrichment and energy injection from type II and type Ia supernovae have been implemented in the multiphase gas model of Scannapieco et al. (2005, 2006). This model has previously

been used to study the formation both of large disk galaxies (Scannapieco et al. 2008, 2009), and of dwarf spheroidal galaxies (Sawala et al. 2010). In Sections 4.1 to 4.5, we briefly explain the most important characteristics of this code, and refer the interested reader to the above references for a more detailed description.

4.1   Gravitational Softening

In order to reduce two-body interactions arising from the particle representation of the matter distribution, the gravitational potential is modified by replacing the divergent $1/r^2$ dependence with $1/(r^2 + \epsilon^2)$, where ϵ is the gravitational softening scale (Aarseth 1963). The choice of ϵ represents a compromise between the errors due to residual two-body effects, and the loss of spatial resolution below several softening scales. We begin our simulations with a softening length fixed in comoving coordinates to 1/10th of the mean interparticle spacing for each particle type, corresponding to $\sim 1h^{-1}$ kpc in the high resolution region. After the collapse of the halo, we keep the softening scale in this region constant in physical coordinates from $z = 7$, at a value of 155 pc. Power et al. (2003) give a lower limit $\epsilon_{acc} = r_{200}/\sqrt{N_{200}}$ to prevent strong discreteness effects in haloes, which corresponds to ~ 140 pc for a $10^{10} M_{\odot}$ object resolved with $N_{200} \sim 10^5$ particles. We also resimulated one of our haloes, Halo 4, with a physical softening scale of 77.5 pc, and checked that this did not alter the results significantly.

4.2   Cooling and UV Background

Above the hydrogen ionisation temperature of 10^4 K, our gas cooling model is based on metal-dependent cooling functions of Sutherland & Dopita (1993). The model assumes collisional excitation equilibrium, and does not include metal or molecular cooling below 10^4K. In addition, we include Compton cooling, which is the main coolant at high redshift. It depends on the free electron density, as well as on the temperature difference between the gas and the evolving CMB. For this purpose, the ionisation states of H, He, and the free electron number density are computed analytically, following the model of Katz et al. (1996). We have included UV background radiation in our model, which adds a heating term to the net cooling function of the partially ionised gas. In all simulations, the UV background is present from $z = 6$, and its spectral energy distribution and the time evolution of its intensity follow the model of Haardt & Madau (1996). A test simulation of Halo 4 without the UV background produced over twice as many stars by $z = 1$, compared to the simulation which includes UV radiation.

4.3   Star Formation Criteria

Cold gas particles can spawn, or be converted into, star particles, subject to certain conditions. We require the gas particle to be in a region of convergent flow. In addition, we impose a physical density threshold ρ_c on the local gas density. The existence of a threshold for star formation is motivated by observations (e.g. Kennicutt 1989, 1998). Calculations by Quirk (1972) as well as numerical simulations, e.g. by

Katz et al. (1996); Springel & Hernquist (2003); Bush et al. (2008) and others have shown that the observed Kennicutt-Schmidt relation can be reproduced in disk galaxies by imposing a volume density threshold, even though different values are assumed. Koyama & Ostriker (2009) demonstrated with high-resolution simulations of the turbulent interstellar medium that the star formation rate depends only weakly on the choice of ρ_c, and values in the range 0.1 cm^{-3} (Stinson et al. 2009) to 100 cm^{-3} (Governato et al. 2010) can be found in the recent literature. Governato et al. reported better convergence in their high-resolution simulation with a choice of 100 compared to 0.1. In this work, we adopt a value of 10 cm^{-3}. We have also tested a density threshold of 0.1 cm^{-3}, more similar to our own previous work. In this case, star formation starts at higher redshift and is less bursty. For Halo 4, the final stellar mass increases by $\sim 36\%$ with a threshold of 0.1 cm^{-3}. This difference is less than the variance in stellar mass between individual haloes, and does not qualitatively affect the stellar mass-halo mass ratio. The limited effect of ρ_c results from the fact that star formation is mostly self-regulating in our simulations. We also impose a threshold $\rho_g/\overline{\rho_g} \geqslant 10^4$ on the local gas overdensity relative to the cosmic mean, which ensures that star formation only takes place in virialized regions even at very high redshift.

4.4 Star Formation Efficiency

Subject to the constraints described in Section 4.3, the star formation efficiency is regulated by a single efficiency parameter $c_\star$, so that the star formation rate density is given by $\dot{\rho}_\star = c_\star \rho_g t_{\mathrm{dyn}}^{-1}$, where t_{dyn} is the local gas dynamical time. The creation of an individual stellar particle of mass $m_\star$ from a gas particle of mass m_g during the time interval Δt is stochastic, with probability given by:

$$p_\star = \frac{m_g}{m_\star} \left[1 - \exp\left(- c_\star \frac{\Delta t}{t_{\mathrm{dyn}}} \right) \right]$$

In simulations with radiative transfer, Gnedin et al. (2009) found that dust acts as a catalyst for molecular cloud formation, suggesting that star formation may be less efficient in the low metallicity environment of dwarf galaxies. As our simulations cannot follow cloud formation, we do not take this into account and assume a constant $c_\star$. Ricotti et al. (2002) showed that if star formation is strongly self-regulating, the star formation rate is determined primarily by the thermodynamic properties of the gas and depends only very weakly on $c_\star$. This result was confirmed in our previous work (Sawala et al. 2010), and in all simulations presented here, we adopt our earlier value of $c_\star = 0.05$.

Each star particle is produced with a single stellar population, whose metallicity is inherited from the parent gas particle. We assume a Salpeter initial mass function (Salpeter 1955), and calculate stellar luminosities using the stellar synthesis model of Bruzual & Charlot (2003).

4.5 Multiphase Interstellar Medium and Feedback

For each star particle, we determine the rate as well as the yields of supernovae type II and type Ia. Chemical yields are calculated separately for the two types, following Woosley & Weaver (1995) and Thielemann et al. (1993), respectively. Supernovae type II are assumed to be instantaneous, while supernovae type Ia follow a uniform delay time distribution between 100 Myrs and 1 Gyr. We assume a constant energy production of 7×10^{50} ergs per supernova, which is released into the interstellar medium (ISM) as thermal energy.

The multiphase scheme of Scannapieco et al. (2006) allows an overlap of diffuse and dense gaseous components. This preserves the multiphase structure characteristic of the ISM, in which components with very different temperatures and densities coexist. It also avoids the overestimation of density in diffuse gas near high density regions which can cause a serious underestimate of its cooling time. The decoupling is achieved by considering as neighbours in the SPH smoothing kernel only gas particles with similar thermodynamical properties, as defined by the ratio of their entropic functions.

Supernova energy is shared equally between the hot and cold phases. Cold particles which receive supernova feedback accumulate energy until their thermodynamic properties are comparable to those of their local hot neighbours. At this point, the energy is released and the particles are promoted to the hot phase. We supplement Scannapieco et al. (2006) by including a seeding mechanism that defines reasonable properties for the local hot phase, even if no neighbouring particles are considered hot at the time. A cold gas particle which has received sufficient supernova energy to raise its thermodynamic properties to this level can thus be promoted, even if it currently has no hot neighbours. This ensures that the distribution of supernova feedback is not delayed at the earliest stages of star formation, when the entire interstellar medium can be in a cold and dense configuration (see Figure 3). The seeding mechanism does not create heat artificially and conserves energy. We have checked that the amount of gas required to seed the hot phase is small, and that the ensuing evolution of the two phases is consistent.

5 GALAXY FORMATION

The different merger histories of the dark matter haloes described in Section 3 are reflected in their gas accretion histories, and in the evolution of the galaxies that form within them. Section 5.1 describes the co-evolution of the halo and its galaxy, while Section 5.2 discusses the properties of the final objects.

5.1 Galaxy Evolution

The halo assembly histories vary significantly, both among our selected sample and among the total population of $10^{10} M_\odot$ haloes. As shown in Figure 2, haloes 3 and 6 had recent major mergers at $z = 0.32$ and $z = 0.21$, respectively, whereas haloes 1 and 2 experienced their last major mergers around $z = 1$. Haloes 4 and 5 have not undergone any major mergers since before $z = 2$. Halo 5 is also significantly more massive compared to the other haloes at high redshift.

The six panels in Figure 3 show the gas mass bound to each of the six haloes as a function of redshift. While the total coloured area indicates the total amount of gas
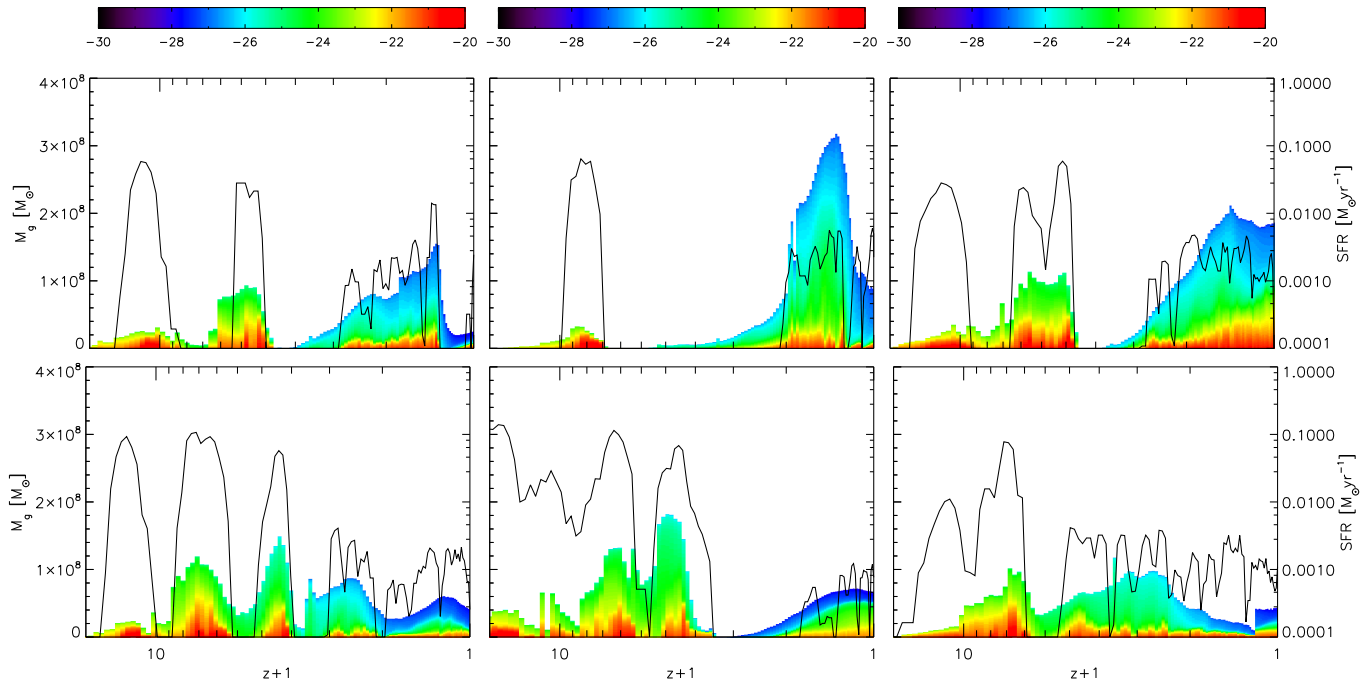
Figure 3. Evolution of total gas mass and star formation rate as a function of redshift. The top row shows, from left to right, haloes 1-3, while the bottom row shows haloes 4-6. The coloured area indicates the total amount of gas in each halo in units of $M_\odot$, corresponding to the scale on the left. The colour coding indicates the differential amount of gas at a given mass density in units of g cm^{-3}, as denoted by the colour bars above. Overplotted in black is the star formation rate as a function of redshift, in units of $M_\odot$ yr^{-1}, corresponding to the scale on the right. In each halo, star formation is tightly coupled to the amount of dense gas, and occurs in bursts, often separated by several 100 Myrs, and associated both with supernova feedback and with mergers. Halo 5 assembles earlier than the five others, and its significantly higher mass at early times leads to a more prolonged starburst in the galaxy contained within it. All galaxies are star-forming at $z = 0$.

in each halo, the star formation rate in the main progenitor, overplotted in black, depends on the presence of cold and dense gas, shown in red and orange colours. We find that two different mechanisms lead to a burstiness of star formation in our simulations. On timescales of hundreds of Myrs, self-regulation of star formation and supernova feedback lead to periodic variations in the gas density, and periodic star formation behaviour. This confirms the earlier results of Pelupessy et al. (2004), Stinson et al. (2007), Mashchenko et al. (2008), Valcke et al. (2008) and Revaz et al. (2009). In addition, gas-rich mergers can induce starbursts. These bursts are irregular and can be separated by several Gyrs. For example, the star formation episodes in Halo 4 beginning at $z = 8$, 4.3 and 2.1 are preceded by mergers at $z = 8.5$, 4.7 and 2.4 with haloes of 2×10^8, 3×10^8 and $10^9 M_\odot$, respectively, which bring in fresh gas. Observations of periodic bursts lasting several hundred million years have been reported for three dwarf galaxies by McQuinn et al. (2009), while a number of dwarf galaxies (Leo I (Dolphin 2002), Leo A (Cole et al. 2007), IC 10 (Cole 2010), IC 1613 (Skillman et al. 2003), DDO 210 (McConnachie et al. 2006) and Carina (Koch et al. 2006)) show extended, quiescent periods between star formation epochs. Cole (2010) suggest mergers and gas accretion as triggers for star formation, but note that individual bursts and mergers can no longer be linked observationally after several Gyrs.

The star formation history of each individual galaxy

in our simulations reflects a combination of internal self-regulation via supernova feedback, and the supply of fresh gas via accretion and mergers. These two effects largely determine the variance in stellar mass between the haloes in our simulations; while differences in merger histories increase the variance, self-regulation via feedback decreases it. In our sample of six haloes of equal final mass, the galaxy stellar masses vary by about a factor of two.

Gas-rich mergers after $z = 6$ imply that the progenitors did not lose all their gas due to the UV background. In our simulations, such mergers occur with haloes that would reach masses above $\sim 10^9 M_\odot$ by $z = 0$. Sawala et al. (2010) showed that at this mass, a combination of UV and supernova feedback removes gas efficiently, while UV radiation alone is not always sufficient. Observations of local group dwarf spheroidals (e.g. Monelli et al. 2010) also suggest that reionisation had at most a minor effect on these galaxies.

Some major mergers also contribute stars. The fraction of final stellar mass formed outside of the main progenitor ranges from $\sim 5\%$ in Halo 5, accreted at $z = 5.2$, to close to 40% for Halo 1, resulting from two major mergers at $z = 3.4$ and $z = 0.8$. Haloes 2 and 6 both accrete $\sim 25\%$ in mergers at $z = 0.4$ and 1, respectively, while haloes 3 and 4 accrete $\sim 7\%$ in mergers at $z = 0.5$ and $z = 2.4$. Since haloes 3, 4 and 5 follow a more typical assembly history, we expect the typical fraction of stars formed outside the main progenitor

Table 2. Overview of numerical simulation results

Halo	$M_\star$ $[10^7 M_\odot]$	M_g $[10^7 M_\odot]$	M_{DM} $[10^9 M_\odot]$	$r_{1/2}$ [kpc]	$\sigma_\star$ [km s^{-1}]	$L_\star$ [km s^{-1}kpc]	Z_{MM}
1	7.81	2.81	9.41	0.87	21	1.4	0.77
2	5.25	6.23	8.34	0.39	17	0.7	0.96
3	4.94	19.4	8.80	0.28	15	1.1	2.65
4	8.14	4.17	8.98	0.36	19	0.4	2.37
5	10.2	7.11	9.94	0.74	33	19	5.17
6	6.17	5.07	8.54	0.68	18	0.3	0.38

Notes: Col. 2: Stellar mass, Col. 3: Gas mass, Col. 4: Dark matter mass (all measured inside r$_{200}$ at $z = 0$), Col. 5: Stellar half-mass radius, Col. 6: De-projected 1-D RMS stellar velocity dispersion, Col. 7: Specific stellar angular momentum L = $|\mathbf{r} \times \mathbf{v}|$ ($\sigma_\star$ and L$_\star$ measured within 3 kpc), Col. 8: Redshift of last major merger (progenitor mass ratio $< \ 3:1$).

in dwarf galaxies of $M_\star \sim 10^8 M_\odot$ to be $< 10\%$, albeit with possible exceptions.

In general, we find that the mean metallicity evolves with age, indicating the recycling of enriched gas in subsequent generations of stars. At each stellar age, we also find a spread in metallicities, which indicates the incorporation of fresh material. However, we note that due to a lack of diffusive metal mixing, the metallicity spread in our simulated stellar populations can be as high as 3 dex, which is larger than observed.

5.2 Galaxy Properties

Several properties of the six simulations are listed in Table 2. They appear to be in broad agreement with the previous studies discussed in Section 2. The final baryon fraction of the haloes are between 1.1 and 2.7 % of the total matter. The final stellar masses of the six galaxies fall between 4.9×10^7 and $1.0 \times 10^8 M_\odot$, which corresponds to stellar mass to total mass ratios in the range of $\sim \ 5 \times 10^{-3} - 10^{-2}$. All galaxies are star-forming at $z = 0$.

The final gas masses vary from 2.8×10^7 to $1.9 \times 10^8 M_\odot$. Observed dwarf galaxies of this stellar mass typically have a substantial HI content (e.g. Staveley-Smith et al. 1992; Geha et al. 2006; de Blok et al. 2008). In our simulations, we cannot directly measure the amount of HI gas. Defining the cold gas as the total amount of gas at temperatures below the peak of the cooling curve and correcting for the contribution of helium and metals, we derive approximate upper limits for the HI masses between 10^7 and $1.2 \times 10^8 M_\odot$. We adopt the notation of Geha et al. (2006) in defining the HI mass fraction as $f_{HI} = M_{HI}/(M_{HI} + M_\star)$, noting that He, H$_2$, hot gas and metals are neglected in the denominator. We derive upper limits for f_{HI} between 11% and 71% in our six galaxies with a median of 35%. In a sample of 101 flux-selected SDSS dwarf galaxies of similar stellar mass, Geha et al. find a higher mean HI fraction of 60%. However, individual galaxies show a large scatter in f_{HI}, with several as high as 95%, and others with upper limits below 10%.

The range of stellar half-mass radii in our six simulations is 0.28 to 0.87 kpc. This is comparable to the typical values obtained by Geha et al. (2006) for half-light radii (r-band), even though the observed sample also contains a handful with half-light radii greater than 1.5 kpc. We note

that only Halo 5, which has the most quiescent assembly history, contains a galaxy with a rotationally supported stellar disk, as reflected by the specific angular momentum L$_\star$. The other five haloes have more ellipsoidal morphologies and very little rotation. This is in contrast to the result of Governato et al. (2010), who report pristine disk galaxies in both of their simulations, albeit in haloes of 2.0 and $3.5 \times 10^{10} M_\odot$. Observations also suggest that isolated dwarf galaxies of this stellar mass are more frequently disk-like (e.g. Hunter & Elmegreen 2006; Geha et al. 2006). The latter find that 30% of edge-on dwarf galaxies show coherent rotation profiles, a number which drops to 18% when all axis-ratios are included, but this should be considered as a lower limit. In a volume-limited sample, Sánchez-Janssen et al. (2010) report that less than 30% of galaxies with stellar masses of $10^8 M_\odot$ have apparent axis ratios below 0.5, and less than 5% below 0.3. They attribute this flattening to stellar feedback. Compared to these observations, our simulated sample of six haloes is too small to assess the statistical significance of a 1 in 6 result. It should also be noted that the stellar half-mass radii of our galaxies are only resolved with a few softening lengths. Therefore, results on details of the galactic structure from our simulations are inconclusive.

6 STELLAR MASS – HALO MASS RELATION

In Section 3, we explained how we constructed our initial conditions from the parent simulation. Its large volume and high dynamic range allows us to demonstrate that we have resimulated a representative sample of haloes. We can therefore derive implications for the global population of galaxies that form in similar mass haloes, and compare with expectations from matching the observed stellar mass function to the abundance of haloes in a ΛCDM universe.

Assuming a monotonic relationship between stellar mass and maximum halo mass, Guo et al. (2010) have compared the abundance of haloes/subhaloes in the Millennium and Millennium-II Simulations to the observed abundance of galaxies as a function of stellar mass obtained from the SDSS DR-7 by Li & White (2009). The observational sample contains over half a million galaxies at low redshift, and extends down to stellar masses of $10^{8.3} M_\odot$ with very small error bars. The combination of the two very large simulations also leads to very small errors on the theoretical halo abundance. The derived stellar mass to halo mass ratio peaks at $M_{halo} = 10^{11.8} M_\odot$ at a star formation efficiency of about 20%, and decreases both for more massive and for less massive haloes (see Figure 4). The decrease in efficiency at the high mass end is generally attributed to AGN feedback (e.g. Croton et al. 2006; Bower et al. 2006), while the decrease for lower mass haloes is assumed to be due to the increasing efficiency of supernova feedback, and the effect of the UV background. This general behaviour was noted earlier from lower precision data by Navarro & Steinmetz (2000), Yang et al. (2003), Dekel & Woo (2003), Conroy & Wechsler (2009) and Moster et al. (2010).

Following Yang et al. (2003), Guo et al. (2010) adopted the following functional form for the mean stellar mass to
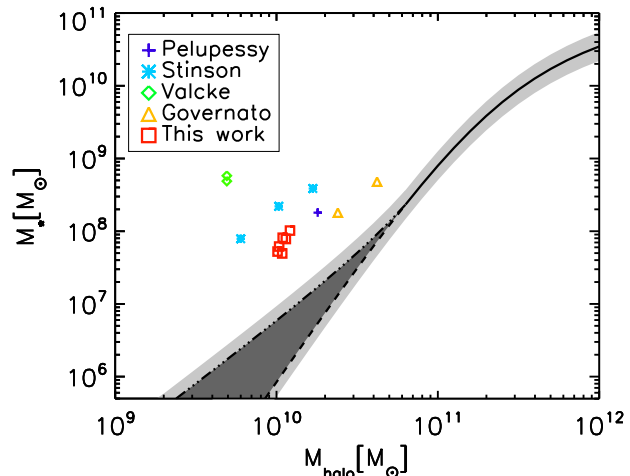
halo mass ratio:

$$\frac{M_\star}{M_{halo}} = c \left[\left(\frac{M_{halo}}{M_0} \right)^{-\alpha} + \left(\frac{M_{halo}}{M_0} \right)^{\beta} \right]^{-\gamma}$$

They report an accurate fit to the data with parameters $c = 0.129$, $M_0 = 10^{11.4}M_\odot$, $\alpha = 0.926$, $\beta = 0.261$ and $\gamma = 2.440$. At the low mass end, the SDSS DR-7 data of Li & White extends to stellar masses of $2 \times 10^8 M_\odot$ with high accuracy, corresponding to a halo mass of $10^{10.8} M_\odot$. Guo et al. extrapolate this relation down to the lowest halo masses resolved in the MS-II. For halo masses of $\sim 10^{10} M_\odot$, this predicts a stellar mass of $\sim 8 \times 10^5 M_\odot$.

From a similar analysis based on SDSS DR-3, which extends to stellar masses of $3.2 \times 10^8 M_\odot$, Moster et al. (2010) also derive a stellar mass – halo mass relation, in good agreement with Guo et al. (2010) at the high mass end. They predict haloes of $10^{10} M_\odot$ to host galaxies with stellar masses of $\sim 5.7 \times 10^6 M_\odot$, significantly higher than found by Guo et al., but still an order of magnitude lower than our hydrodynamical simulations predict. Moster et al. note, however, that such haloes are at best marginally resolved at their mass resolution ($2.8 \times 10^8 M_\odot$), prohibiting a self-consistent treatment of subhaloes. Consequently, they only include haloes above $1.6 \times 10^{10} M_\odot$ in the conditional mass function. Moster et al. also apply their analysis to an analytic Sheth-Tormen mass function obtained by Vale & Ostriker (2006). In this non-parametric model, a halo mass of $10^{10} M_\odot$ corresponds to a stellar mass of $1.9 \times 10^6 M_\odot$, more similar to the value of Guo et al. (2010).

In Figure 4, we plot the stellar mass – halo mass relation of Guo et al. (2010) for haloes between 10^9 and $10^{12} M_\odot$. The solid section of the line shows the relation in the region directly derived from SDSS DR-7 data where the uncertainties are very small. The dashed section denotes an extrapolation to stellar masses below $10^{8.3} M_\odot$, assuming a faint-end slope of $\alpha = -1.15$ for the stellar mass function, as reported by Li & White (2009). Studies of the faint-end of the stellar mass function are either limited to nearby regions or galaxy clusters, or require corrections for incompleteness and, in the case of photometric redshifts, background subtraction, which introduce considerable uncertainties (e.g. Christlein et al. 2009). As a result, different values for α in the range of -1.1 to -1.6 are found in the recent literature (e.g. Trentham et al. 2005; Blanton et al. 2005; Carrasco et al. 2006; Baldry et al. 2008). The dark grey area in Figure 4 shows the effect of a steepening of the faint-end slope up to $\alpha = -1.58$, the value reported by Baldry et al. (2008). While this has a strong effect on the lowest mass haloes, we note that it cannot account for the discrepancy we find in haloes of $10^{10} M_\odot$. In order to fit the constraints of SDSS DR-7, the maximal dispersion at fixed halo mass is 0.2 dex in $M_\star$, indicated by the light-grey area. We overplot the results of our six simulations as red squares and add other $z = 0$ predictions from the studies listed in Table 1, correcting all halo masses for baryonic effects, as described below. It is apparent that all these hydrodynamical simulations overproduce stellar mass for their respective halo mass by at least an order of magnitude.

In Table 3, we compare the properties of our six simulations to the abundance matching predictions. We note that, due to the outflow of baryons, the total mass of our six haloes is almost a factor of $1 - \Omega_b/\Omega_m$ smaller than the masses of

Figure 4. The stellar mass – halo mass relation, derived by Guo et al. (2010), compared to the results of several numerical simulations. The solid black line denotes the range constrained by the SDSS DR-7 data, while the dashed line is an extrapolation to lower masses, with a faint-end slope of -1.15 for the stellar mass function. The dark grey area shows the influence of a steeper faint-end slope up to -1.58 (dash-dotted line), while the light grey area represents the maximally allowed dispersion of 0.2 dex in $M_\star$ for a given halo mass. The coloured symbols denote the results of hydrodynamical simulations, as listed in Table 1 and Table 2, excluding simulations that did not evolve to $z = 0$ or assume a baryon fraction of 1% *ab initio*. The red squares indicate our own six simulations. For consistency, we use the halo masses of the pure dark matter simulations for our own simulations, and apply a correction of 20% to all other haloes, where this information is not available. All hydrodynamical simulations overpredict the stellar mass with respect to the observed relation by more than an order of magnitude.

the corresponding haloes from the pure dark matter simulation. This effect is expected at such low star formation efficiency. For consistency with Guo et al. (2010), we therefore use the (higher) peak masses of the pure dark matter simulations in deriving the stellar mass predicted for each of our haloes by the abundance matching argument. For all galaxies listed in Table 1 whose peak halo mass cannot be defined or is not given, we increase the halo mass in Figure 4 by $\Omega_b/\Omega_m \sim 20\%$, the maximally expected correction.

Comparing the results of our simulations to the predictions, we find that the hydrodynamical simulations overproduce stellar mass by a median factor of ~ 50. Alternatively, abundance matching predicts that galaxies of $10^{7.9} M_\odot$, the median stellar mass produced in our hydrodynamical simulations, should reside in haloes with typical masses of $\sim 4.5 \times 10^{10} M_\odot$, rather than $10^{10} M_\odot$. If $10^{10} M_\odot$ haloes really hosted galaxies with $M_\star = 10^{7.9} M_\odot$, a ΛCDM universe would overpredict their abundance by a factor of ~ 4.

This discrepancy is too large to be attributed solely to incompleteness in the observed stellar mass function. Baldry et al. (2008) have used the stellar mass – surface brightness relation of SDSS galaxies in order to estimate the completeness at the faint end. Based on this analysis, Li & White (2009) estimate the completeness at $10^{8.3} M_\odot$ to be well above 70%. Following Baldry et al., the uncer-

Table 3. Comparison of stellar mass – halo mass ratios

Halo	$M_\star$ $[10^7 M_\odot]$	M_{tot} $[10^9 M_\odot]$	M_{max} $[10^9 M_\odot]$	$M_\star$(SMF) $[10^7 M_\odot]$
1	7.81	9.52	12.1	0.154
2	5.25	8.46	11.2	0.1216
3	4.94	9.04	10.7	0.104
4	8.14	9.10	11.8	0.143
5	10.2	10.1	12.5	0.171
6	6.16	8.65	10.7	0.104

Notes: Col. 2: Stellar mass obtained from simulation, Col. 3: Combined mass (m_{200}) of stars, gas & dark matter of the halo in the hydrodynamical simulation, Col. 4: Peak halo mass (m_{200}) in the pure dark matter simulation, Col. 5: Stellar mass corresponding to M_{max} from the abundance matching.

tainty in the number of $10^{7.9} M_\odot$ galaxies is much smaller than the discrepancy we report.

The difference is also unlikely to be attributable to numerical errors in our hydrodynamical simulations, or to the specific parametrisation of star formation and feedback in our model. From Table 1, it is clear that all other current hydrodynamical models, while succeeding in reproducing many of the observed features of individual dwarf galaxies, also predict similar or higher galaxy mass to halo mass ratios. They thus also fail to reproduce the low star formation efficiencies required to explain the observed abundances of dwarf galaxies in a ΛCDM universe.

Haloes of $10^{10} M_\odot$ are well resolved in the Millennium-II Simulation, and the number of such haloes in a volume of 137^3 Mpc^3 is clearly large enough for statistical uncertainties to be small. While the assumed cosmological parameters of $\Omega_\Lambda = 0.75$, $\Omega_m = 0.25$ and $\sigma_8 = 0.9$ are only marginally consistent with the five-year WMAP data (Komatsu et al. 2009), this has a negligible effect on the mass function. It is unlikely that the number density of $10^{10} M_\odot$ haloes formed in a ΛCDM cosmology is significantly overestimated in our parent simulation. A lower value of σ_8 would slightly *increase* the abundance of haloes of this mass, but as Yang et al. (2003) have shown, the abundance matching result, which depends on the cumulative abundance of more massive haloes, is almost unchanged at $10^{10} M_\odot$ in ΛCDM.

In warm dark matter (WDM) models, structure is erased below a characteristic free-streaming length that depends on the assumed properties of WDM particles. Zavala et al. (2009) have compared the halo mass functions in high resolution dark matter simulations of ΛCDM and ΛWDM, assuming $m_{\rm WDM} = 1$ keV, and find that the present-day abundance of haloes of $10^{10} M_\odot$ decreases by a factor of ~ 3. These simulations truncate the power spectrum of the initial conditions in the WDM case but neglect thermal velocities, which could increase the effect. However, recent combined analysis of structures observed in the Lyman-α forest of SDSS and HIRES by Viel et al. (2008) suggest a lower limit of ~ 4 keV for thermal relics in a pure ΛWDM cosmology, which would allow only a much smaller deviation from CDM on these scales. While a WDM model could thus perhaps account for the reported discrepancy between simulations and star formation efficiencies inferred from abundance matching, the required WDM particle mass

appears disfavoured by observation. A WDM solution would also significantly alter the internal structure of dwarf haloes, and simultaneously reduce the abundance of lower mass objects.

In principle, one could turn to direct measurements of halo masses for individual galaxies on the relevant scales, to elucidate whether the halo mass function of the ΛCDM model, and the inferred stellar mass – halo mass relationship, are correct. Direct mass estimates, through gravitational lensing (e.g. Mandelbaum et al. 2006) are only available for haloes with masses above $\sim 10^{11.8} M_\odot$, however, where they agree with the CDM predictions and the relationship of Guo et al.. For dwarf galaxies, one has to rely on HI rotation curves (e.g. de Blok et al. 2008), which do not give reliable estimates for *total* halo masses.

As demonstrated in Section 3, we have been careful to resimulate a representative sample of haloes, and to exclude any systematic bias. Considering the limited variance in stellar mass among the six haloes, statistical fluctuations are an unlikely source for the discrepancy.

It is worth noting that semi-analytical models of galaxy formation (e.g. Kauffmann et al. 1993; Cole et al. 2000) attempt to reproduce the observed faint-end slope of the stellar mass function in a ΛCDM universe by assuming highly efficient supernova feedback in small haloes (e.g. Benson et al. 2003; Khochfar et al. 2007). We have applied the semi-analytic model of Guo et al. (2010, b), which reproduces the Li & White (2009) stellar mass function, to the merger trees of our six resimulated haloes, and also to a randomly selected sample of similar mass haloes from the Millennium-II Simulation. We find no difference in the predicted stellar mass between the selected haloes and the random sample, but stellar masses that are roughly two orders of magnitude smaller than in our hydrodynamical simulations. Independent of the cause of the discrepancy between the hydrodynamical simulations and the observed stellar mass function, there is thus a divergence between current hydrodynamical and semi-analytical models for dwarf galaxies. The semi-analytical models are tuned to produce the correct galaxy abundance, whereas hydrodynamical models aim at reproducing the physical processes and the structure of individual galaxies. Clearly, these two aspects cannot be treated separately, if we are to converge to a consistent picture of galaxy formation.

7 SUMMARY

We have performed high-resolution hydrodynamical simulations of six $\sim 10^{10} M_\odot$ haloes, extracted from a large, cosmological parent simulation. We find that differences in merger histories lead to the formation of dwarf galaxies with different star formation histories and final stellar masses between 4.9×10^7 and $10^8 M_\odot$. These stellar masses agree with previous simulations of similar mass haloes, and the structure of our simulated galaxies resembles that of observed galaxies of similar stellar mass, to the extent which we can resolve structure in our simulations.

However, all these simulations imply an efficiency of conversion of baryons into stars which is at least an order of magnitude larger than that which is required to explain the observed abundance of dwarf galaxies in a ΛCDM uni-

verse. While current hydrodynamical simulations, including our own, are consistent with almost arbitrarily high mass-to-light ratios for the faintest galaxies in haloes of $10^9 M_\odot$ or less, they thus appear to be inconsistent with the mass-to-light ratios of larger dwarf galaxies, even when a moderately steep faint-end slope of the stellar mass function is assumed. The current recipes for mechanisms such as UV heating and supernova feedback appear sufficient to remove the "Missing Satellites Problem" for the smallest satellites. However, isolated dwarf galaxies with stellar masses of $10^8 M_\odot$ are still substantially overproduced in current hydrodynamical simulations, even when these mechanisms are included.

Our results suggest three possible explanations: The current observational count of dwarf galaxies could be incomplete, underestimating the true number density of $10^8 M_\odot$ galaxies by a factor of four or more. In that case, the hydrodynamical simulations could be correct, but the semi-analytical models that produce low abundances of dwarf galaxies have been tuned to incorrect data.

If the count of dwarf galaxies is almost complete at $10^8 M_\odot$, these galaxies must, in a ΛCDM universe, be residing in haloes significantly more massive than $10^{10} M_\odot$, and all current hydrodynamical simulations overpredict the efficiency of star formation by more than a factor of ten. This could be an indication of numerical problems, or, more likely, of incorrect or incomplete assumptions about the relevant astrophysics. Several possible mechanisms may contribute to a star formation efficiency in current simulations that is too high compared to real galaxies:

• Supernova feedback may be more efficient in ejecting gas from dwarf galaxies than current hydrodynamical simulations predict. For example, Guo et al. (2010, b) showed that the observed stellar mass function can be reproduced in semi-analytic models by assuming very strong mass-loading of winds in low mass haloes.

• The full effect of reionisation on the IGM may not be captured in current models. As a result, cooling times may be underestimated, and the fraction of gas-rich mergers overestimated. Local sources of extreme UV and soft X-ray radiation may also ionise the interstellar medium, inducing another self-regulation mechanism for star formation (Ricotti et al. 2002; Cantalupo 2010).

• Low dust content may lead to less efficient cloud formation and shielding at low metallicities. The transformation rate of cold gas into stars, currently assumed to be universal, may therefore be overestimated in dwarf galaxy simulations (Gnedin et al. 2009).

• Processes such as magnetic fields, cosmic rays and the feedback from population-III stars are not included in any of the current models, and may further reduce the star formation efficiency.

Any revised model would however still have to reproduce features of individual galaxies consistent with observations. We also note that a model which substantially decreases the number of $10^8 M_\odot$ galaxies would imply that the halo masses of fainter dwarf galaxies would need to be revised upwards, as some of these would now be required to live in $10^{10} M_\odot$ haloes.

If the observed stellar mass function is complete, and the hydrodynamical simulations correctly capture the relevant physics of galaxy formation, the Millennium-II Simulation (and similar ΛCDM simulations) overpredict the number of $10^{10} M_\odot$ dark matter haloes. This would seem to require the underlying physical assumptions of the ΛCDM model to be revised. Warm Dark Matter may offer a possibility, but only for particle masses of ~ 1 keV, below the limit apparently implied by recent Lyman-α observations.

Of the three proposed scenarios, it appears that missing astrophysical effects in the simulations are the most likely cause of the discrepancy, and the most promising target in search of its resolution. While the three scenarios differ in nature, none is without significant implications for galaxy formation, which will have to be addressed in the future.

REFERENCES

Aarseth S. J., 1963, MNRAS, 126, 223

Baldry I. K., Glazebrook K., Driver S. P., 2008, MNRAS, 388, 945

Belokurov V., Walker M. G., Evans N. W., Gilmore G., Irwin M. J., Just D., Koposov S., Mateo M., Olszewski E., Watkins L., Wyrzykowski L., 2010, ArXiv e-prints

Benson A. J., Bower R. G., Frenk C. S., Lacey C. G., Baugh C. M., Cole S., 2003, ApJ, 599, 38

Blanton M. R., Lupton R. H., Schlegel D. J., Strauss M. A., Brinkmann J., Fukugita M., Loveday J., 2005, ApJ, 631, 208

Bower R. G., Benson A. J., Malbon R., Helly J. C., Frenk C. S., Baugh C. M., Cole S., Lacey C. G., 2006, MNRAS, 370, 645

Boylan-Kolchin M., Springel V., White S. D. M., Jenkins A., Lemson G., 2009, MNRAS, 398, 1150

Bruzual G., Charlot S., 2003, MNRAS, 344, 1000

Bush S. J., Cox T. J., Hernquist L., Thilker D., Younger J. D., 2008, ApJ, 683, L13

Cantalupo S., 2010, MNRAS, 403, L16

Carrasco E. R., Mendes de Oliveira C., Infante L., 2006, AJ, 132, 1796

Chapman S. C., Peñarrubia J., Ibata R., McConnachie A., Martin N., Irwin M., Blain A., Lewis G. F., Letarte B., Lo K., Ludlow A., O'neil K., 2007, ApJ, 662, L79

Christlein D., Gawiser E., Marchesini D., Padilla N., 2009, MNRAS, 400, 429

Cole A. A., 2010, Publications of the Astronomical Society of Australia, 27, 234

Cole A. A., Skillman E. D., Tolstoy E., Gallagher III J. S., Aparicio A., Dolphin A. E., Gallart C., Hidalgo S. L., Saha A., Stetson P. B., Weisz D. R., 2007, ApJ, 659, L17

Cole S., Lacey C. G., Baugh C. M., Frenk C. S., 2000, MNRAS, 319, 168

Conroy C., Wechsler R. H., 2009, ApJ, 696, 620

Croton D. J., Springel V., White S. D. M., De Lucia G., Frenk C. S., Gao L., Jenkins A., Kauffmann G., Navarro J. F., Yoshida N., 2006, MNRAS, 365, 11

de Blok W. J. G., Walter F., Brinks E., Trachternach C., Oh S., Kennicutt R. C., 2008, AJ, 136, 2648

Dejonghe H., de Zeeuw T., 1988, ApJ, 333, 90

Dekel A., Silk J., 1986, ApJ, 303, 39

Dekel A., Woo J., 2003, MNRAS, 344, 1131

Diemand J., Kuhlen M., Madau P., 2007, ApJ, 667, 859

Dolphin A. E., 2002, MNRAS, 332, 91

Efstathiou G., 1992, MNRAS, 256, 43P

Ferrara A., Tolstoy E., 2000, MNRAS, 313, 291

Geha M., Blanton M. R., Masjedi M., West A. A., 2006, ApJ, 653, 240

Gnedin N. Y., Tassis K., Kravtsov A. V., 2009, ApJ, 697, 55

Governato F., Brook C., Mayer L., Brooks A., Rhee G., Wadsley J., Jonsson P., Willman B., Stinson G., Quinn T., Madau P., 2010, Nature, 463, 203

Guo Q., White S., Boylan-Kolchin M., De Lucia G., Kauffmann G., Lemson G., Li C., Springel V., Weinmann S., 2010, ArXiv e-prints

Guo Q., White S., Li C., Boylan-Kolchin M., 2010, MNRAS, 404, 1111

Haardt F., Madau P., 1996, ApJ, 461, 20

Hoeft M., Yepes G., Gottlöber S., Springel V., 2006, MNRAS, 371, 401

Hunter D. A., Elmegreen B. G., 2006, ApJS, 162, 49

Jenkins A., 2010, MNRAS, pp 172–+

Katz N., Weinberg D. H., Hernquist L., 1996, ApJS, 105, 19

Kauffmann G., White S. D. M., Guiderdoni B., 1993, MNRAS, 264, 201

Kennicutt Jr. R. C., 1989, ApJ, 344, 685

Kennicutt Jr. R. C., 1998, ApJ, 498, 541

Khochfar S., Silk J., Windhorst R. A., Ryan Jr. R. E., 2007, ApJ, 668, L115

Klypin A., Kravtsov A. V., Valenzuela O., Prada F., 1999, ApJ, 522, 82

Koch A., Grebel E. K., Wyse R. F. G., Kleyna J. T., Wilkinson M. I., Harbeck D. R., Gilmore G. F., Evans N. W., 2006, AJ, 131, 895

Komatsu E., Dunkley J., Nolta M. R., Bennett C. L., Gold B., Hinshaw G., Jarosik N., Larson D., Limon M., Page L., Spergel D. N., Halpern M., Hill R. S., Kogut A., Meyer S. S., Tucker G. S., Weiland J. L., Wollack E., Wright E. L., 2009, ApJS, 180, 330

Koposov S., Belokurov V., Evans N. W., Hewett P. C., Irwin M. J., Gilmore G., Zucker D. B., Rix H., Fellhauer M., Bell E. F., Glushkova E. V., 2008, ApJ, 686, 279

Koyama H., Ostriker E. C., 2009, ApJ, 693, 1316

Larson R. B., 1974, MNRAS, 169, 229

Li C., White S. D. M., 2009, MNRAS, 398, 2177

Mandelbaum R., Seljak U., Kauffmann G., Hirata C. M., Brinkmann J., 2006, MNRAS, 368, 715

Martin N. F., Ibata R. A., Irwin M. J., Chapman S., Lewis G. F., Ferguson A. M. N., Tanvir N., McConnachie A. W., 2006, MNRAS, 371, 1983

Mashchenko S., Wadsley J., Couchman H. M. P., 2008, Science, 319, 174

McConnachie A. W., Arimoto N., Irwin M., Tolstoy E., 2006, MNRAS, 373, 715

McQuinn K. B. W., Skillman E. D., Cannon J. M., Dalcanton J. J., Dolphin A., Stark D., Weisz D., 2009, ApJ, 695, 561

Monelli M., Hidalgo S. L., Stetson P. B., Aparicio A., Gallart C., Dolphin A. E., Cole A. A., Weisz D. R., Skillman E. D., Bernard E. J., Mayer L., Navarro J. F., Cassisi S., Drozdovsky I., Tolstoy E., 2010, ApJ, 720, 1225

Moore B., Ghigna S., Governato F., Lake G., Quinn T., Stadel J., Tozzi P., 1999, ApJ, 524, L19

Moster B. P., Somerville R. S., Maulbetsch C., van den Bosch F. C., Macciò A. V., Naab T., Oser L., 2010, ApJ, 710, 903

Navarro J. F., Steinmetz M., 2000, ApJ, 538, 477

Pelupessy F. I., van der Werf P. P., Icke V., 2004, A&A, 422, 55

Power C., Navarro J. F., Jenkins A., Frenk C. S., White S. D. M., Springel V., Stadel J., Quinn T., 2003, MNRAS, 338, 14

Quirk W. J., 1972, ApJ, 176, L9+

Revaz Y., Jablonka P., Sawala T., Hill V., Letarte B., Irwin M., Battaglia G., Helmi A., Shetrone M. D., Tolstoy E., Venn K. A., 2009, A&A, 501, 189

Ricotti M., Gnedin N. Y., Shull J. M., 2002, ApJ, 575, 49

Salpeter E. E., 1955, ApJ, 121, 161

Sánchez-Janssen R., Méndez-Abreu J., Aguerri J. A. L., 2010, MNRAS, 406, L65

Sawala T., Scannapieco C., Maio U., White S., 2010, MNRAS, pp 3–+

Scannapieco C., Tissera P. B., White S. D. M., Springel V., 2005, MNRAS, 364, 552

Scannapieco C., Tissera P. B., White S. D. M., Springel V., 2006, MNRAS, 371, 1125

Scannapieco C., Tissera P. B., White S. D. M., Springel V., 2008, MNRAS, 389, 1137

Scannapieco C., White S. D. M., Springel V., Tissera P. B., 2009, MNRAS, 396, 696

Simon J. D., Geha M., 2007, ApJ, 670, 313

Skillman E. D., Tolstoy E., Cole A. A., Dolphin A. E., Saha A., Gallagher J. S., Dohm-Palmer R. C., Mateo M., 2003, ApJ, 596, 253

Somerville R. S., 2002, ApJ, 572, L23

Springel V., 2005, MNRAS, 364, 1105

Springel V., Hernquist L., 2003, MNRAS, 339, 289

Springel V., Wang J., Vogelsberger M., Ludlow A., Jenkins A., Helmi A., Navarro J. F., Frenk C. S., White S. D. M., 2008, MNRAS, 391, 1685

Springel V., White S. D. M., Jenkins A., Frenk C. S., Yoshida N., Gao L., Navarro J., Thacker R., Croton D., Helly J., Peacock J. A., Cole S., Thomas P., Couchman H., Evrard A., Colberg J., Pearce F., 2005, Nature, 435, 629

Staveley-Smith L., Davies R. D., Kinman T. D., 1992, MNRAS, 258, 334

Stinson G. S., Dalcanton J. J., Quinn T., Gogarten S. M., Kaufmann T., Wadsley J., 2009, MNRAS, 395, 1455

Stinson G. S., Dalcanton J. J., Quinn T., Kaufmann T., Wadsley J., 2007, ApJ, 667, 170

Sutherland R. S., Dopita M. A., 1993, ApJS, 88, 253

Thielemann et al. 1993, Origin and Evolution of the Elements. Cambridge Univ. Press, p. 299

Tollerud E. J., Bullock J. S., Strigari L. E., Willman B., 2008, ApJ, 688, 277

Trentham N., Sampson L., Banerji M., 2005, MNRAS, 357, 783

Valcke S., de Rijcke S., Dejonghe H., 2008, MNRAS, 389, 1111

Vale A., Ostriker J. P., 2006, MNRAS, 371, 1173

Viel M., Becker G. D., Bolton J. S., Haehnelt M. G., Rauch M., Sargent W. L. W., 2008, Physical Review Letters, 100, 041304

Woosley S. E., Weaver T. A., 1995, ApJS, 101, 181

Yang X., Mo H. J., van den Bosch F. C., 2003, MNRAS, 339, 1057

Zavala J., Jing Y. P., Faltenbacher A., Yepes G., Hoffman Y., Gottlöber S., Catinella B., 2009, ApJ, 700, 1779